Nonuniformity correction and thermal drift compensation of thermal infrared camera

Olivier Riou, Stephane Berrebi, Pierre Bremond

reprint: Proceedings of the SPIE, Volume 5405, p. 294-302 (2004)

Non Uniformity Correction and thermal drift compensation of thermal infrared camera

Olivier Riou

Centre d'études et de recherche de thermique et d'environnement des systèmes (CERTES), Université Paris XII, IUT de Sénart, avenue Pierre Point, 77127 Lieusaint

Stéphane Berrebi, Pierre Brémond

CEDIP Infrared Systems, 19 boulevard Georges Bidault F-77 183 Croissy-Beaubourg

Corresponding author: **olivier.riou@u-pec.fr**
Version: **Monday, August 21, 2023**

Abstract. In the last decade, a technology of thermal imagers based on new infrared detectors has been developed for both civil and military applications. These imagers implement miniaturized infrared detectors arranged in a matrix in the optical focal plane of the imager. FPA's technology links the detector matrix to specific electronics that allow detection and addressing at each pixel. This technology has allowed a rapid improvement in the performance of thermal imagers. Nevertheless, its use in thermographic measurement requires some metrological care. The first problem is the uniformity of the pixel response and the stability of this uniformity over time. The second problem is the compensation of the thermal drift. In this paper we present some practical solutions developed by CEDIP infrared systems to perform non-uniformity and thermal drift corrections. Performance and limitations are discussed.

https://doi.org/10.1117/12.547807

1. Introduction

Infrared thermography provides a non-contact, full-field, efficient and fast method for real-time surface temperature measurements. Infrared cameras, which are thermographic sensors, consist of focal plane array, Dewar, flexible programmable miniaturized drive electronics with analog to digital converters and high speed digital video image processors. The processors allow real-time non-uniformity correction for visualization or recording. The proliferation of focal plane array technology has allowed a significant improvement in sensitivity. Today, NETD close to 20 mK is becoming the standard, allowing the application range of thermography to be expanded. However, certain applications require higher spatial resolution of temperature. Let's mention aeronautical applications characterized by small spatial variations of temperature, the inverse methods using exact gradient temperature, the characterization of the radiation pattern of an antenna or the observation of strain fields on a structure. One of the other major difficulties with thermography is that temperatures are not measured directly. The temperature is calculated from the incoming radiation measured at the detector. This received radiation consists of radiation emitted not only from the object, but also from the surroundings, from the atmosphere and/or windows, and from inside the camera (lens and thermal imager itself). Thermal drifts result from the instability of the lens and camera temperatures and must be corrected to improve the accuracy of the measurements. The aim of this paper is to present solutions for non-uniformity correction and drift compensation for high-end research and development applications.

2. Characteristics of Infrared Emission

The infrared camera is based on the passive absorption of thermal radiation. Thus, it is possible to visualize a scene in the infrared spectrum or to measure the number of photons emitted (flux) and, depending on the modeling of the emitter (and its environment), to deduce the temperature of the emitter. Flux is a function of space and time variables.

Radiant emission is usually treated in terms of the black body concept. Its monochromatic emissive power (spectral exitance) of the black body is [1]:

$$M^0(\lambda, T) = \frac{2\pi hc^2}{\lambda^5} \times \frac{1}{\exp\left(\frac{hc}{\lambda kT}\right) - 1} \ [W\ m^{-3}] \tag{1}$$

Assuming that the source is Lambertian [2], The detectable spectral radiant power L^0 is depending on the solid angle of view Ω [sr] of the detector:

$$L^0(\lambda, T) = \frac{M^0(\lambda, T)}{\pi}$$
$$L^0(\lambda, T) = \frac{2hc^2}{\lambda^5} \times \frac{1}{\exp\left(\frac{hc}{\lambda kT}\right) - 1} \ [W\ m^{-2} m^{-1} sr^{-1}] \tag{2}$$

The detectable flux ϕ^0 is simply derivate from Eq. 2 by dividing by the photon energy $\varepsilon = h\,c/\lambda$:

$$\phi^0(\lambda, T) = c_1 \times \frac{\lambda^{-4}}{\exp\left(\frac{c_2}{\lambda T}\right) - 1} \ [\text{photons}\ s^{-1} m^{-2} m^{-1}\ sr^{-1}]$$
$$c_1 = 2c = 6\ 10^8 \ [\text{photons}\ s^{-1}\ m\ sr^{-1}] \tag{3}$$
$$c_2 = \frac{hc}{k} = 1.4388\ 10^{-2}\ K\ m$$

The majority of thermal cameras operate in three windows of atmospheric transmission: the windows 1.5-2.5 µm (SWIR, short wave infrared), 3-5 µm (MWIR, medium wavelength infrared) and 8-12 µm (LWIR, long wavelength infrared).

In table 1, we present the characteristics of emission of 300 K black body temperature. We will call here "thermal contrast" the ratio of the flux variation corresponding to a variation of 1°C of the target temperature normalized to the flux value at 300K.

Spectral band	Radiative power $L^0(T)$ @300 K	Number of emitted photons $\Phi^0(T)$ @300K	$\Delta\Phi^0(T)/\Delta T$	Contrast
µm	W m^{-2} sr^{-1}	photons s^{-1} m^{-2} sr^{-1}	photons s^{-1} K^{-1} m^{-2} sr^{-1}	% K^{-1}
[1.5µm; 2.5µm]	$8.4\ 10^{-4}$	$1\ 10^{16}$	$7\ 10^{14}$	7%
[3µm; 5µm]	1.8	$4\ 10^{19}$	$1.5\ 10^{18}$	4%
[8µm; 12µm]	38.5	$1{,}9\ 10^{21}$	$3.1\ 10^{19}$	2%

Table 1. Characteristics of emission independently of any detection

The flux/noise ratio is also affected by the choice of the spectral band. If N is the number of photons, the photon noise varies as $N^{-0.5}$which is to be considered only for BLIP detectors. Thus, the flux/noise ratio decreases with spectral band and appears more favorable for the thermographic measurements in the 8-12 µm band.

3. Characteristics of FPAs using in IR measurements

3.1. Photosignal

In photovoltaic detection, a detector transforms the flux in an electric output (voltage or current). The photosignal is spatially and time dependent. The photosignal will depend on the characteristics of absorption of the FPA detectors: the spectral band, the surface of detection A_D, the quantum efficiency $QE(\lambda)$ and the solid angle of detection $d\Omega$. The conversion of the flux $\phi^0(\lambda, T)$ into photosignal is specified in relation 4:

$$\text{photosignal}\ (T,t) = A_D \times d\Omega \int_{\lambda_1}^{\lambda_2} QE(\lambda) \times\ \phi^0(\lambda, T)\ d\lambda \quad [W] \tag{4}$$

Because of numerous parameters involved in Eq. 4, each detector gives a specific photosignal which would differ from the other. Note that $d\Omega$ depends on the optical number n (indicated by the optical aperture f/n of the camera): the flux absorbed by the detector for an optical opening f/1 is more important than in f/2, etc… In practice, the reduction in flux according to the optical number can be technologically compensated by a spectral band (a detector MCT 3.7-4.9 µm at f/2 produces a photo-signal equivalent to an InSb detector 3.7-5.1 µm at f/3).

Note that the photosignal provided by the bolometric detection have the same structure of Eq. 4 if we consider the absorption efficiency $R(\lambda)$ instead of the quantum efficiency and the black body radiance $L^0(\lambda, T)$ instead of the detectable flux $\phi^0(\lambda, T)$ [3].

https://doi.org/10.1117/12.547807

3.2. Digital thermosignal

The digital thermosignal corresponds to the energy absorbed by the detector during the integration time τ. In a simple case, this energy varies both with τ and the photosignal according to the following relation:

$$\text{Energy (T)} = \int_{\tau} photosignal\,(T,t)\,dt \approx \overline{photosignal(T)} \times \tau \quad [\,\text{J}\,] \tag{5}$$

We suppose implicitly that the photosignal is constant during integration time. The energy is then converted numerically into digital thermosignal during the reading process. Integration time τ appears then to be the main adjustable parameter to optimize the digital thermosignal to noise ratio. It is the same concerning the bolometric detection technology.

The NUC process states on the linear variation of digital thermosignal with flux. We test successfully the linearity for a FPA MWIR-InSb in a standard measurement situation, using a black body emitter. The results are showed in figure 1 for several integration times and black body temperatures.

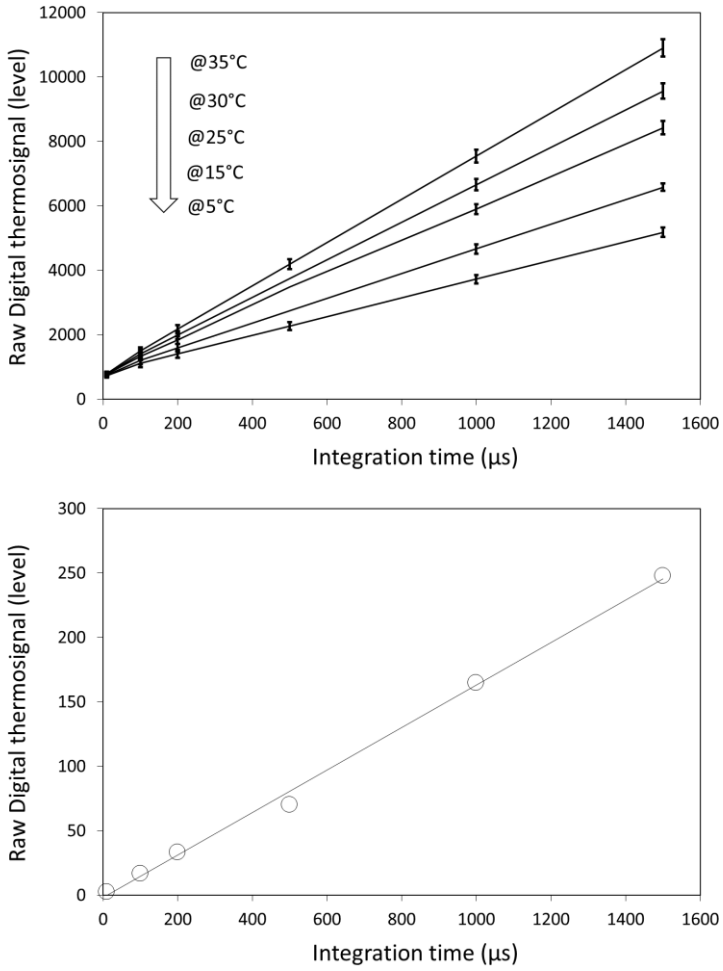

Figure 1 Digital thermosignal versus integration time of a MWIR-InSb FPA at constant black body emitter temperature. For each temperature, we evaluate the mean value (line) and the standard deviation σ (error bars) of 320×256 pels. Raw digital thermosignals corresponds to 10, 100, 200, 500, 1000 and 1500 µs integration times. Raw digital thermosignals are obtained before NUC process. The offset is set to 700 levels.

A small non-linearity is observed for lower integration times ($\tau < 100\mu s$). Offset is due to insensitivity to low flux (photo-signal limited by the darkness current) and saturation to high flux level or to large integration times. Integration time also affects the sensitivity of the FPA. Sensitivity shows a linear behavior with τ (see Fig. 1). The Level range/sensitivity ratio corresponds to a single temperature range. Notes that temperature range depends also on integration time.

3.3. Point element (Pel)

In practice, only the Digital thermosignal (DL) remains accessible to the user. The elementary point (Pel) which integrates the functions of detection, time integrating and reading, gives the digital thermosignal. DL is the unit response one gets from each detector after the time integrating and reading process. DL is to be distinguished both from the photosignal provided by the detector and from the pixel used in the picture.

3.4. Sensitivity

For a detector which produces an electrical current, the ratio current (in Ampere)/photovoltaic power (in Watt) defines responsivity. It is the same for the detectors which produce a voltage. From a practical point of view, we prefer the concept of "sensitivity Pel" defined by the Level to black body temperature change ratio. It is expressed in Level/°C and is obtained in the calibration process.

3.5. From Pel to Pixel

The main stages of the process are represented in the Figure 2. The exposure provides a photo-signal whose characteristic flux-temperature is intrinsically nonlinear. The reading of the photo-signal gives the digital thermosignal on which one carries out numerically the evaluation of the Bad elements. Then we proceed to the NUC and thermal drift correction before getting to the pixel.

3.6. BLIP limit

Once the BLIP limit is reached, the technological dispersion of Pels around an average behavior induces a fixed spatial noise figure, which is assumed to be sufficiently invariant to be corrected from characterization data. In photovoltaics, the BLIP limit in NETD Pel can be estimated to be around 10 mK (@300K, f/1, 8-12µm). A statistical study carried out over the period 1999-2003 on LWIR-MCT and MWIR-InSb photovoltaic imagers shows that this limit has now been reached on commercial arrays (Figure 3)

The statistical dispersion is larger for MCT than for InSb. InSb is a highly stable covalent semiconductor whose technology has been mastered very early. LWIR MCT technology, a less stable semiconductor, is constantly improving and has now reached a level equivalent to MWIR InSb.

https://doi.org/10.1117/12.547807

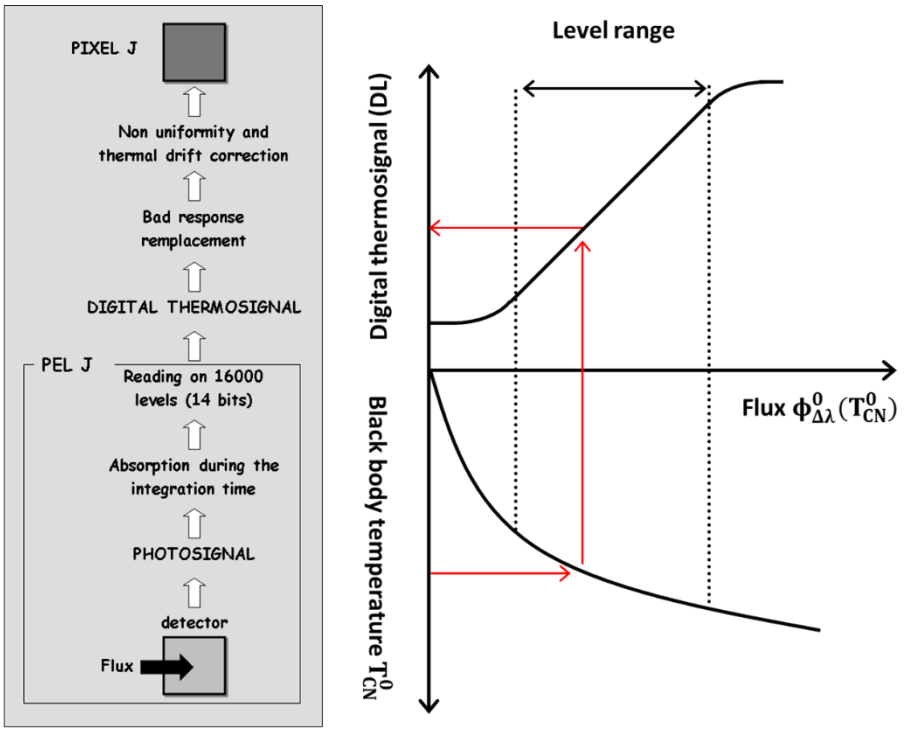

Figure 2. Steps of thermal imagery. A radiometric measurement provides a photosignal and its integrating and reading provide a digital thermosignal. The Pel integrates the functions of detection, integration and reading. The dynamic range is evaluated by the level range on which the digital thermosignal is proportional with flux. The temperature range is obtained by dividing the level range by the average sensitivity of the FPA

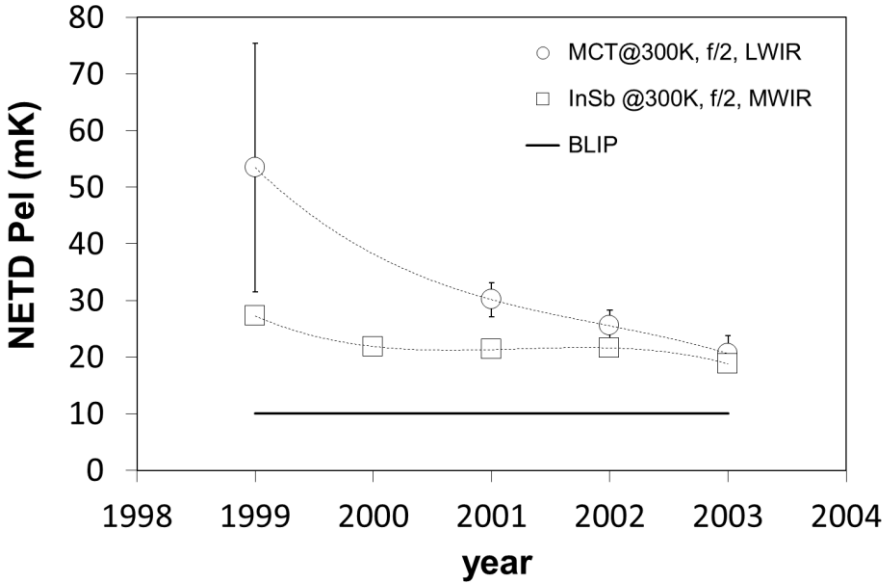

Figure 3. Comparison of the NETD Pel evolution of commercial matrices LWIR-MCT and MWIR-InSb. The NETD Pel is given at 25°C. For each imager, it is obtained by dividing the average residual spatial noise after NUC by the sensitivity. The bars show the statistical dispersion of the imagers tested over the period 1999-2003 (12 MCT and 20 InSb). CEDIP data.

https://doi.org/10.1117/12.547807

4. Specific Problems of FPA detectors

Any FPA camera uses a great number of Pels. Each Pel gives a digital thermosignal different from the other one. The matrix presents then a specific problem of uniformity of response for a uniform thermal scene. One characterizes this non-uniformity by the Fixed Pattern Noise (FPN).

4.1. The causes of the fixed pattern noise

Fixed pattern noise expresses mainly the non-uniformities of conversion of the flux to the digital thermosignal. This is due to the disparities in the metrological characteristics of each Pel. The sources of FPN are numerous. Let us quote the principal ones:

- Product quality of the FPA. Their production implements the techniques of micro-electronics. Any variations in size or quality of the semiconductor will involve disparities in metrological characteristics of the Pels,
- Thermal regulation. It is essential to maintain constant the temperature of the FPA. Small variations are difficult to avoid. They have a variable impact on the offset, sensitivity and noise of the Pels,
- Electronic interface and the multiplexing of the photo-signal. Electronics generate a fixed space noise. The images can be affected by a random structure, a structure of grid (technology CMOS) or line (technology CCD),
- Electronic noise (1/f noise). The 1/f noise is present in any semiconductor device. It comes from the interfaces semiconductor-insulator, which gives to noise an irreducible character. It limits the sensitivity at the low levels and the exactitude of the procedures of non-uniformity correction,
- Optics. Fixed pattern noise can be caused by the optics of the camera. Optics can generate non uniformity in the illumination of the FPA. Results are a decrease of intensity at the edges or generation of circular geometrical disparities.

It isn't possible to control each source of FPN. It is only possible to proceed to corrections. During the correction process, one regards the camera as an operational device, taking account of all the internal sources of fixed noise.

4.2. Defects of the matrices

Defects of the matrices are due to local alterations of wafer used in FPA manufacture. These defects lead to the degradation of the Pels. One is brought to distinguish their metrological properties:

- Pels of which the sensitivity is zero and NETD is infinite
- Pels which present an offset or a sensitivity very large
- Damage Pels which answer correctly but whose NETD exceeds the average NETD

The first are blind, the second limits the dynamic range of measurement, and the third provides a degraded pixel. It is essential to identify them before carrying out their elimination. The operational qualification of each Pel is made by the camera assembler during a calibration process. The test for detection "bad Pel" is based on information of offset, sensitivity and temporal noise. In practice, we define limits compatible with the 14 bits digit thermosignal range. A too high sensitivity reduces the temperature range. A low sensitivity Pel degrades the NETD while the temporal noise limits the detectivity.

https://doi.org/10.1117/12.547807

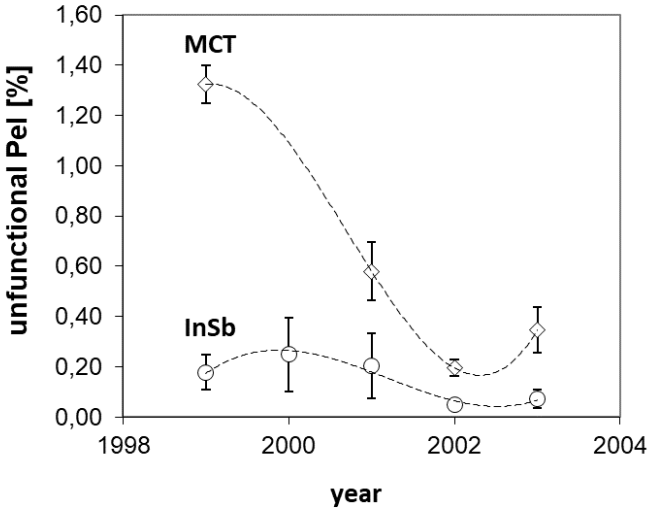

Figure 4. Trend of the number of reformed Pels in MCT-LWIR and InSb-MWIR arrays since 1999. The test criteria are a deviation of $\pm 25\%$ in sensitivity, $\pm 30\%$ in offset and pel noise greater than 7-10 levels out of 16000. The failure rate in 2002 was 1.5 ‰. CEDIP data.

5. Non uniformity correction

Insofar as the camera is stable, fixed space noise is in theory invariant in time and can be corrected. The procedure of NUC presented below is based on the algorithm of Shulz [4].

5.1. Calibration process

The calibration consists in correlating the digital thermosignal to the black body temperature. One carries out a calibration using a black body which one varies the temperature. For each temperature of calibration, one records the associated DL. The characteristic DL-temperature of the black body defines the calibration curve of the detector. The infrared imager includes a great number of Pels which it is necessary to distinguish from each other. In the continuation, the DL associated with a Pel will be represented by DL_{ij}. The Index i $(1 < i < n)$ indicates the temperatures of the black body T_i^0 used in the calibration while the index j $(1 < j < N)$ refers to N pels. In the calibration, DL of each pel of the FPA is measured for various temperatures of the black body. One defines an average $\langle DL_i \rangle$ associated with the black body temperature T_i^0:

$$\langle DL_i \rangle = \frac{\sum_{j=1}^{N} DL_{ij}(T_i^0)}{N} \quad (6)$$

It is not necessary to explicit the mathematical function of the calibration curve: we use flux as variable. Associating the DL with flux, we obtain a linear average characteristic. The individual DL deviates from the average characteristic because of non-uniformities and temporal noise. The non-uniformity process consists to bring the individual characteristic to the average characteristic. Non-uniformity results in distortion DL_{ij} compared to the average value:

$$\Delta DL_{ij} = DL_{ij} - \langle DL_i \rangle \quad (7)$$

A polynomial function fits the distortion:

$$\Delta DL_{ij}^{lsq} = a_j + b_j \times \langle DL_i \rangle + c_j \times \langle DL_i \rangle^2 \quad (8)$$

a_j is the offset and b_j the normalized sensitivity or gain (the gain b_j=0 when an individual digital thermosignal equals the mean digital thermosignal). For a correction of offset, only aj is calibrated. For a linear correction, a_j and b_j are calibrated. The quadratic correction introduces a third term c_j, etc. The degree of correction is arbitrary. All these parameters are evaluated and memorized for each pel of the sensor. The residual distortion is obtained by subtracting the adjusted variation from the individual one:

$$\Delta \mathrm{DL}_{\mathrm{ij}}^{\mathrm{c}} = \mathrm{DL}_{\mathrm{ij}} - \Delta \mathrm{DL}_{\mathrm{ij}}^{\mathrm{lsq}} \tag{9}$$

The residual distortion is due mainly to the average temporal noise and thermal drift. The corrected pixel is then determined by the following relations:

$$\begin{aligned} \Delta \mathrm{DL}_{\mathrm{ij}}^{\mathrm{c}} &= \mathrm{DL}_{\mathrm{ij}} - \mathrm{a}_{\mathrm{j}} \ (\text{Offset correction}) \\ \Delta \mathrm{DL}_{\mathrm{ij}}^{\mathrm{c}} &= \frac{\mathrm{DL}_{\mathrm{ij}} - \mathrm{a}_{\mathrm{j}}}{1 + b_j} \ (\text{Gain correction}) \end{aligned} \tag{10}$$

In practice, we are satisfied with a linear correction. Two points in temperature are enough to determine the parameters gain and offset. The calibration temperatures used are generally 20°C and 100°C. The higher limit is imposed by the normal use conditions of an extended black body. On the operator level, offset and gain calibration are possible. In standard situation, only offset calibration is required. It is done starting from only one external reference.

5.2. Current NUC parameters

Current NUC parameters allow setting various parameters for the active NUC table:

- The Integration time. Integration time is the amount of time in microsecond the detectors are staring at the target scene during each frame period. This is analogous to exposure time of a film camera where a faster shutter speed is used for brighter scenes and a longer integration time for scene with less light,
- Bad pixel parameters. Bad pixel parameters control the threshold that the bad pixel detection algorithm uses to determine the location of the bad pixels during the two-point correction process. Three parameters are used:
    1. Offset threshold. The offset threshold sets an offset range equal to $\pm 30\%$ of the mean offset of all the pixels of the FPA: $\langle \mathrm{a_i} \rangle = \sum_{\mathrm{j}} \mathrm{a_{ij}}/\mathrm{N}$. Pixel offset which doesn't fit in this limit would not be considered as operational,
    2. Sensitivity threshold. The sensitivity threshold is set to $\pm 25\%$ to the mean sensitivity $\langle \mathrm{b_i} \rangle = \sum_{\mathrm{j}} \mathrm{b_{ij}}/\mathrm{N}$. If a given pixel sensitivity is less than the low percent number, the pixel is considered as blind,
    3. Noise Threshold. The noise threshold is set to $\pm 3\overline{\sigma}_{\mathrm{i}}$ of the deviation of average residual standard deviation $\overline{\sigma}_{\mathrm{i}}$ in DL unit. Average is obtained from n tests at fixed black body temperature $\mathrm{T_i^0}$. Pel which exhibits noise larger than $\pm 3\overline{\sigma}_{\mathrm{i}}$ is considered as bad.
- FPA window size. This parameter controls the FPA widowing parameters that apply for a given NUC. All CEDIP camera FPAs have the capability to readout user determined area of the FPA that is less than its full size (1/2 or1/4 size). The smaller the area that is read out, the faster the frame rate of the system can be.

5.3. Performance of NUC process

The results of the NUC process are presented in Figures 5.

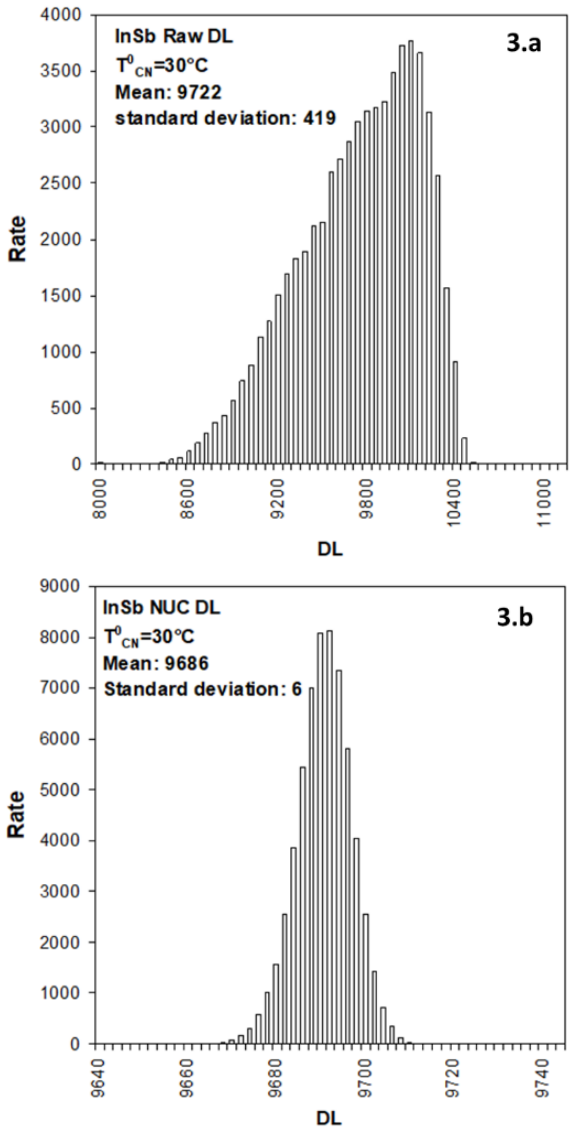

Figure 5. **3a**: raw DL at 30°C. The average sensitivity to this temperature is 419 level/°C for 1500µs integration time @f/2. The standard deviation in temperature is 1.9K (NETD). **3b**: NUC DL at 30°C. The two point NUC are 5°C and 35°C respectively. The NETD image raises the value of 26 mK. The Mean level decrease of 36 levels, inducing an offset of temperature of 0.15°C.

5.4. Non Uniformity Correction limits

The suppression of the fixed pattern noise finds tree limits:

- non-linearity of distortion ΔDL_{ij},
- the temporal stability of the sensitivity $\langle b_i \rangle$ and offset $\langle a_i \rangle$
- the Thermal drift.

A small non-linearity, negligible when average behavior is studied, can be important when one considers differences, as is the case in the correction of NUC. In theory, the variations of linearity can be treated by corrections of a higher nature, inducing mathematical relations more complex and difficult to

digitize (division, extraction of root…), an application software development and a significant computing time. These corrections are not implemented in standard imagery. It should be noted that a correction of degree higher than 3 does not have an analytical solution (a simplified method taking account of the non-linearity of the digital thermosignal is presented in [5]).We tested the residual distortion of the NUC digital thermosignal of 3 Pels randomly selected among the 320×240 Pels of a MWIR-InSb matrix. The result is presented in Figure 6.

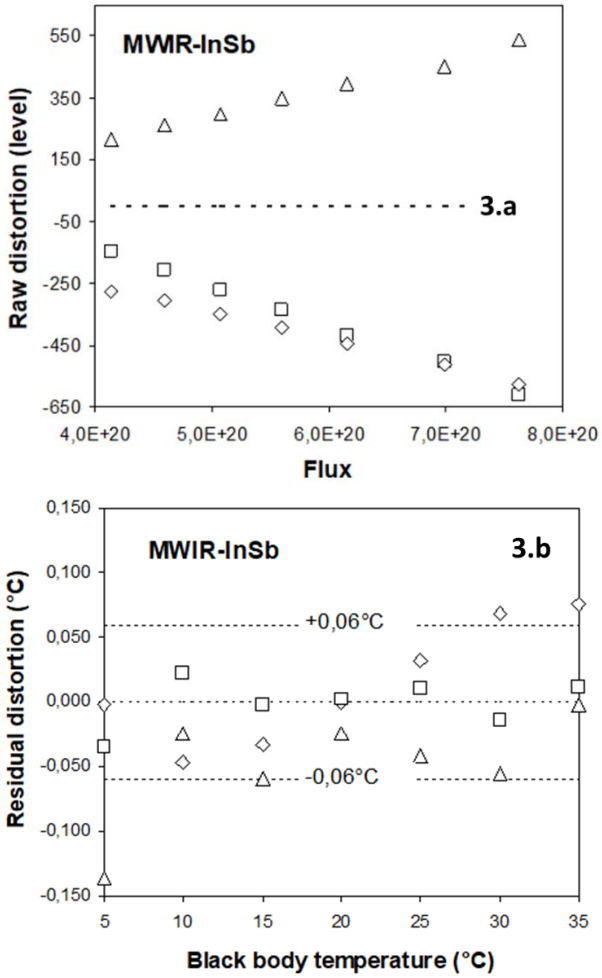

Figure 6. Correction of the fixed pattern noise. On left, variation of the raw distortion versus photon flux (Eq. 3) before NUC (dotted line: zero average distortion). On right, residual distortion which are calculated from NUC offset and gain (a_j and b_j) of tree random Pels of 320×240 MWIR-InSb FPA. NUC process is performed at 5°C and 35°C.

The NETD Pixel masks a metrological reality: it gives a statistical order of magnitude of the residual space noise but does not allow quantifying dispersion in the digital level of individual Pel. before correction of non-uniformity, Peak to peak residual spatial variations ($\pm 3\sigma$) is about 3K (Fig.6a) to 60mK (Fig.6b).

The correction of the NUC assumes that the sensitivity and offset are constant over time. We present in Table 2 an evaluation of the stability of the FPA [6]. The matrices are characterized and corrected. The efficiency of the NUC is then followed over time. The time of stability is defined by the NEDT pixel remaining below the NETD Pel. The NETD image masks a metrological reality: it gives a statistical order of magnitude of the residual space noise but does not allow quantifying dispersion in the digital level. After

https://doi.org/10.1117/12.547807

correction of NUC, Peak to peak residual spatial variations is about 120mK or 20mK RMS. The correction of NUC supposes sensitivity and offset constant with time. We present on table 2 an evaluation of the stability of the FPA [7]. The matrices are characterized and corrected. NUC is then followed in time. The time of stability is defined by $\text{NEDT image} \leq \text{NETD pel}$

FPA	PtSi Bolometric 640×486	InSb Photovoltaïc 256×256	HgCdTe Photovoltaïc 128×128	Unit
Spectral band	3 - 5	3 - 5	8 - 12	µm
NETD PEL	57	20	21	mK
NETD image	11	11	19	mK
Time of stability	$\gg 25$	≈ 1	< 0.2	Hour

Table 2. Examples of temporal stability

MWIR-PtSi bolometric FPA has the stability of a silicon technology (time stability more than 25 hours). MWIR-InSb photovoltaïc FPA uses a binary compound with stable covalent crystal should be corrected every one hour. LWIR-MCT photovoltaïc FPA uses ternary compound with the weak ionic bond, should be corrected every approximately ten minutes.

6. Thermal drift correction

After Non Uniformity Calculation and Bad Pixel Replacement, infrared cameras are calibrated with a Black Body. Calibration includes the set of operations which establish, under a specified configuration (Filter, integration time), the relationship between value indicated by the camera (in DL) and the corresponding known value of the standard (Temperature of the Black Body).

One of the major problems is that temperature is not measure directly. The incident radiation on the detector is first measured. This received radiation consists of radiation emitted not only from the target but also from the camera itself. Radiation is also attenuated by the lens and filter of the sensor. During the calibration the Back body radiation is fixed while internal radiation changes. The following figure illustrates the sources of radiation received by a sensor:

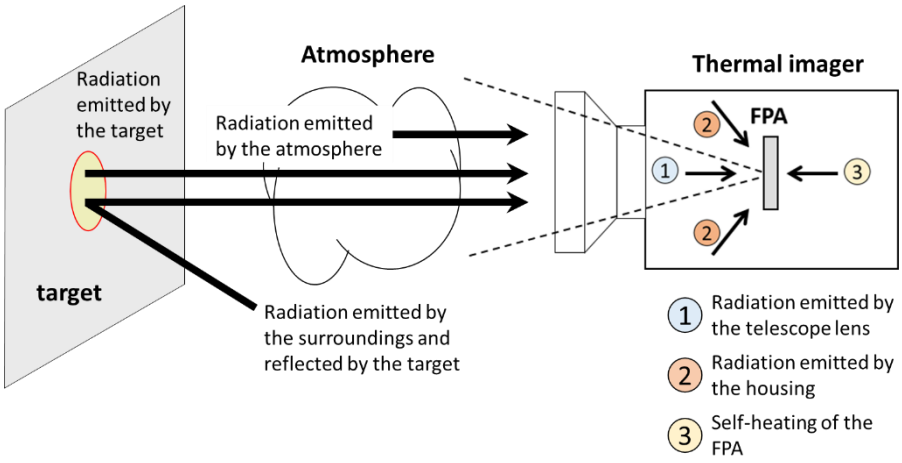

Figure 7. Radiation contributions in a general measurement situation.

Compensation deals with radiation coming from the camera housing, its own optics (including lens and internal filter) and the embedded electronics. To emphasis the importance of an accurate compensation for this, the error without compensation of internal radiation is plotted in figure 8. The MWIR camera configuration includes an internal filter (3.9µm) and an integration time (300µs). The error is +/-15°C at 350°C (Black body temperature) while the ambient temperature changes in 160 minutes from 10°C to 35°C.

However very few thermal imagers are properly compensated and consequently the measured object temperature will be dependent on the temperature of the imager. The radiation from the imager itself is a consequence of the fact that all optical elements attenuate the object radiation and therefore also emit radiation due to their own temperature. The method used to achieve the compensation for this is to use an internal temperature measurement and process the digital signal in real time in the camera. Thermocouple positions are precisely determined after a set of tests. Sensitivity versus error should be maximum relationships for real time processing the simplest.

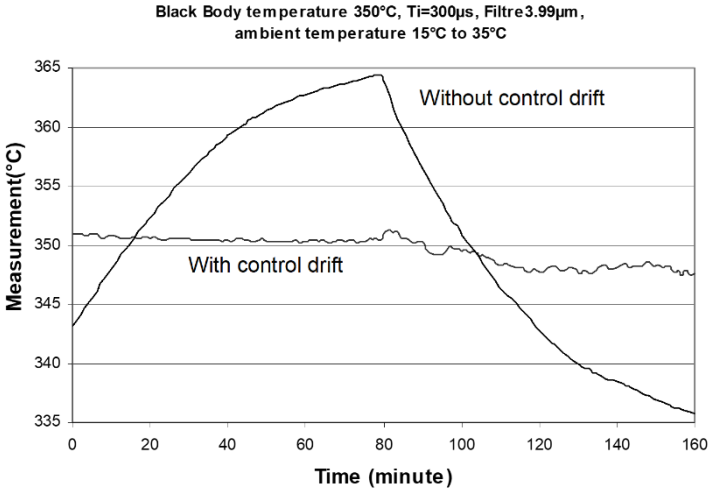

Figure 8. Temperature measurement with and without drift control.

As a difference with old compensation methods, gain and offset are evaluated for each calibration point. Variations could be caused by a number of reasons e.g. radiation from optics between the object and the detector, different background radiation on detector, filters and varying transmissions due to lens transmission. The telescope lens needs additional thermocouple. This technique is available for every configuration (with or without filter) and for the complete set of optic components from object to detector. Other advantages of the technique that we propose are:

- No need to use a calibration curve inside of the camera. The infrared camera always produces a value proportional to irradiance,
- Allows the final user to perform his own calibration (including thermal drift compensation) by only collecting calibration data and internal temperature measurement.

The result of thermal drift control is shown in Figure 8, where the error is limited to +/-4°C under normal operating conditions (variation in ambient temperature and prolonged use).

https://doi.org/10.1117/12.547807

7. Conclusion

We studied the metrological chain between the photosignal and the pixel. We showed that the spatial resolution in temperature obtained after correction of NUC is of the same order of magnitude as the NETD Pel. This performance satisfies the majority of the users who don't need a resolution better than 6×NETD (dispersion peak to peak). This limitation primarily poses problems for applications in aeronautics, the inverse methods using exact gradient temperature, the characterization of the radiation pattern of an antenna or the observation of strain fields in structure etc… where the phenomena are fast and of low amplitudes. The problem of thermal drift is presented. Thermal drift is compensated for temperatures of camera from -10°C to +40°C. In this range, the residual drift remains smaller than +/-4°C.

References

[1] Thermal insulation - Heat transfer by radiation – Vocabulary International Organization for Standardization. 2022 NF EN ISO 9288.

[2] Gilbert Gaussorgues (1999). La thermographie infrarouge, Principes - Technologies – Applications. Éditeur : Tec et Doc – Lavoisier. ISBN 10 : 2743002905

[3] Tissot, J.L., Trouilleau, C., Fieque, B. et al (2006). Uncooled microbolometer detector: recent developments at ULIS. Opto-Electron. Rev. 14, 25–32 (2006). https://doi.org/10.2478/s11772-006-0004-2

[4] M. Schulz, L. Caldwell (1995). Nonuniformity correction and correctability of infrared focal plane arrays. Infrared Physics & Technology, Volume 36, Issue 4, Pages 763-777. https://doi.org/10.1016/1350-4495(94)00002-3

[5] Ruizhong Wang, Peiyi Chen, Peihsin Tsien (1998). An improved nonuniformity correction algorithm for infrared focal plane arrays which is easy to implement. Infrared Physics & Technology, Volume 39, Issue 1, Pages 15-21. https://doi.org/10.1016/S1350-4495(97)00034-0

[6] Olivier Riou, Luc Audaire (2001). Panorama technologique des caméras à FPA, atouts et limites. Journées d'études de Thermographie instrumentale et industrielle THERMOGRAM'2001. Editeurs : Institut de la thermographie, Institut universitaire de technologie Sénart-Fontainebleau. ISBN 978-2-9513961-0-4

[7] Leszek Swierkowski and Owen M. Williams (2002). Advanced flood nonuniformity correction for emitter array infrared projectors. Proc. SPIE 4717, Technologies for Synthetic Environments: Hardware-in-the-Loop Testing VII. https://doi.org/10.1117/12.474712